

# Polarization and intensity distributions of refraction halos

G. P. Können

Royal Netherlands Meteorological Institute, P.O. Box 201, NL-3730-AE De Bilt, The Netherlands

Received May 14, 1983

By using Taylor expansions, simple expressions are obtained for the deflection of light by ice crystals. With these simplified formulas, the intensity distributions of halos as a function of scattering angle are calculated analytically near the halo angle. It is found that the intensity distributions of halos depend on the number of degrees of freedom of the generating set of crystals. The differences in the purity of the colors of various types of halo are explained subsequently on the basis of their intensity distributions. An analytical description of the shape of the halo or of the halocaustic near the halo angle is obtained also. On the basis of the obtained intensity distributions, the polarization of refraction halos as a function of scattering angle is calculated, in which both contributions (birefringence of ice and polarization by refraction) are taken into account. It is found that the polarization of parhelia and tangent arcs shows a strong maximum near the inner edge of the halo over an angular range of  $0.1^\circ$ , followed by a similar maximum of reversed polarization at  $0.5^\circ$  from the first one. The  $22^\circ$  halo shows a less strong maximum near its edge over an angular range of  $0.5^\circ$ . Halos at  $46^\circ$  from the sun also show a strong polarization near their inner edges, but the direction of the polarization is perpendicular to the polarization of the  $22^\circ$  halo edges. The possibility for detecting ice crystals on Venus by polarimetry near the halo angle is discussed briefly.

## 1. INTRODUCTION

Two mechanisms determine the polarization of refraction halos: refraction of light by the faces of the crystals (Fresnel refraction) and the birefringence (double refraction) of ice. The effect of Fresnel refraction has been known for many years, and the calculation of this contribution to the polarization of halos is simple. However, the resulting degree of polarization is low, about 4% for the  $22^\circ$  halo group (the  $22^\circ$  halo and its associated arcs and spots) and 16% for the  $46^\circ$  halo group; only the latter polarization is visible to the naked eye if it is equipped with a polarizing filter.

On the other hand, the fact that birefringence in ice crystals contributes significantly to the polarization of halos has become known only recently. It was discovered by accident in June 1977,<sup>1</sup> although the mechanism is quite obvious. Birefringence leads to a splitting of the incident light into two completely polarized light beams, each generating its own halo. The direction of the polarization (E vector) of the two beams is such that they are perpendicular to each other. Because of the (slight) difference in the index of refraction for these polarized beams, the halo angle for each beam also differs. In the case of the  $22^\circ$  halo group, the difference is  $0.11^\circ$ . This means that a halo consists of two completely polarized components, which are slightly shifted from each other (Plate II). At the red inner edge, only one component is visible and the polarization is complete, but, farther away from the sun, the polarization decreases because of the overlapping of the polarized components.<sup>2</sup> So, unlike polarization by Fresnel refraction, birefringence results in a marked structure in the polarization along the halo.

The calculation of polarization by birefringence is more complicated than for Fresnel refraction. Since the polarization results from a shift of two polarized halos, the intensity distribution as a function of scattering angle of the halo has to be known to calculate the polarization.

Because of the complexity of the halo formulas, exact analytic intensity calculations are difficult. For parhelia, White<sup>3</sup>

developed a general formalism and solved it numerically. A similar approach was used by Fraser and Thompson<sup>4</sup> for the sun pillar. Greenler,<sup>5</sup> however, avoided the mathematical problems by using a Monte Carlo method. With this technique, he obtained qualitative intensity distributions of many types of halo. However, none of these authors included polarization in his calculations.

On the other hand, for parhelia, polarization has been calculated by McDowell,<sup>6</sup> but he restricted the formalism to refraction and reflection effects alone. The deflection of light by anisotropic prisms has been treated recently by White<sup>7</sup>; he presented the halo angles for the polarized components of the  $22^\circ$  halo and the  $46^\circ$  halo.

In this paper, the polarization of refraction halos as a function of scattering angle is calculated generally, near the halo angle, taking into account both contributions to the polarization. The required intensity distributions for halos are obtained by approximating the deflection formulas for light in ice crystals near the halo scattering angle. It is shown that, with this approach, the intensity distributions of halos can be expressed in simple analytical functions. A similar technique has been used for the calculation of the intensity distributions of rainbows.<sup>8</sup> For halos the derivation is, in principle, also straightforward, but the number of steps required to reach the answer is rather high. Therefore in this paper we leave some obvious steps to the reader.

The intensity distributions that we derive have a range of validity of at least  $5^\circ$  from the edge of the  $22^\circ$  halo. They can be used to explain the color distributions and the shapes of halos and to calculate their polarization patterns.

The sequence of this paper is as follows. Section 2 and Appendix A define the notation. In Section 3 a classification of halos is given in terms of the degrees of freedom of the generating set of ice crystals. In Section 4 the propositions of our model are defined. In Section 5 the expansion of the deflection functions is performed, and in Section 6 the intensity distributions and the shapes of four familiar halos are calculated. In Section 7 the polarization distributions of these

halos are presented. Section 8 discusses the intensity distributions, color distributions, and polarization distributions of halos. Finally, in Section 9 suggestions are made for further research.

2. NOTATION

No strict convention exists for the notation in halo theory. Most authors follow in main lines the notation of Humphreys,<sup>9</sup> but others (e.g., White<sup>3</sup>) have their own systems. For the sake of uniformity, we should prefer to take over Humphreys' system completely, but in our case this is not entirely possible. The reasons are that our problem encompasses the fields of scattering theory, polarization, and halo theory and that the conventional notation in these three fields cannot be combined. We make the following choice. For the polar coordinates of scattered light  $\theta$  and  $\phi$  are used according to the convention in scattering theory. Humphreys uses  $\Delta$  and  $S$  for his polar coordinates, and Tricker uses  $\Delta$  and  $\sigma$ .<sup>10</sup> Although, when possible, we follow Humphreys' notation, the definition of more angles is required for the specification of the orientation of ice crystals in space, for birefringence and for the expansion of the deflection functions. Appendix A and Fig. 1 summarize our notation for vectors, angles, and scalars.

3. DIMENSIONS OF HALOS AND DEGREE OF FREEDOM OF A CRYSTAL

Ice crystals floating in the atmosphere may be oriented randomly or have a preferential orientation. If a set of randomly oriented crystals becomes gradually preferentially oriented, the shape, the intensity distribution, and the polarization pattern of its generated halos change also.

The orientation of an ice crystal in space is determined by the three angles  $i$ ,  $h$ , and  $q$  (see Appendix A). Thus a crystal may have maximally three degrees of freedom. This is the case if the crystals are oriented randomly. The resulting refraction halos are annuli with the sun at center and are called by Tape<sup>11</sup> three-dimensional halos. If a preferential orientation reduces the degree of freedom from three to two, the halo is called two dimensional. If only one degree of freedom is left, an even higher orientation is present, and the resulting halo is called one dimensional. Obviously, in this case there exist two relations between the three angles determining the orientation of the crystals. The highest orientation should occur if no degree of freedom is left. Such halos should be called zero dimensional. In refraction halos zero-dimensional halos do not exist, but for halos caused by reflection there is an example. This is the subsun.

Table 1 summarizes the properties of halos by their dimensions and gives some typical examples of them among the refraction halos.

Degenerate Halos

In exceptional cases the properties of a halo do not follow Table 1. The most prominent case is the parheliion, a one-dimensional halo. This halo is also a curve, but this curve is degenerate since it is folded back on itself.<sup>12</sup> This results in a line-shaped halo, oriented mainly radially with respect to the light source and with a point-shaped caustic at its point closest to the source. However, such a caustic is in general a characteristic of two-dimensional halos. It turns out that the intensity distribution of the parhelia is identical with the one

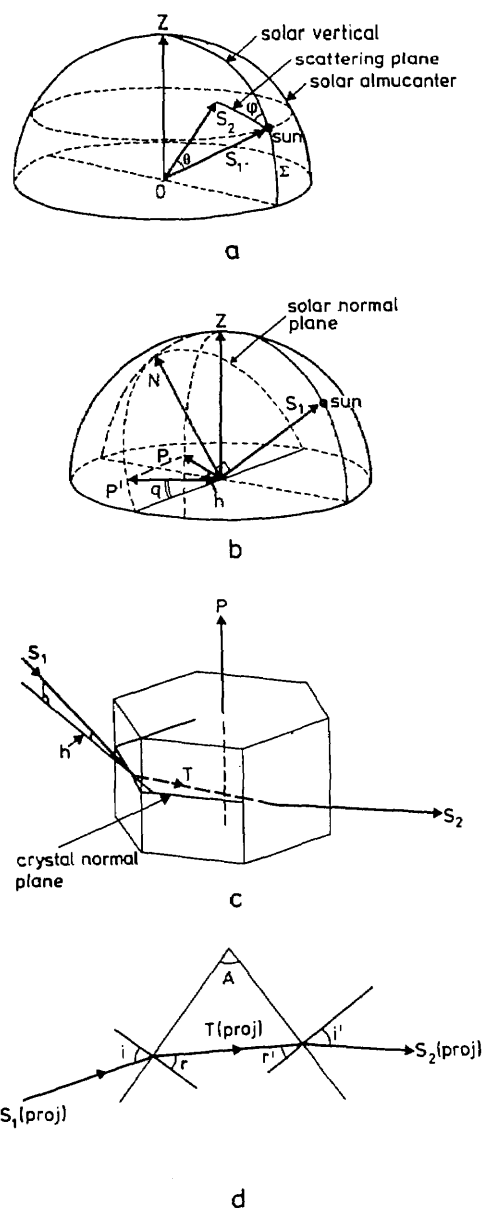


Fig. 1. Definition of vectors, planes, and angles. If the position of the axial vector  $\hat{P}$  of a crystal is fixed in space, the relevant angles can be defined; d refers to the normal plane of a crystal and shows the projection of some vectors in this plane. See Appendix A for the notation.

Table 1. Properties of Halos

Dimension	Appearance	Typical Examples
0	A point	-
1	A curve, mainly perpendicular to the radial direction from the sun	Circumzenithal and circumhorizontal arc; Parry arcs
2	An area, with a caustic usually toward the sun	Upper- and lower-tangent arcs; infralateral arcs
3	Annulus with the sun at center and with a sharp inner boundary	22° halo; 46° halo

**Table 2. Properties of Degenerate Halos**

Dimension	Appearance	Typical Example
1	A line or a curve with a caustic toward the sun	Parhelia
2	An area of infinitely small width, causing the halo caustic to collide with itself	Lower-tangent arc near the subsolar point

of two-dimensional halos (Section 6). A parhelia is called here a degenerate one-dimensional halo.

There exist also degenerate two-dimensional halos. An example is the lower-tangent arc near the subsolar point. Here the degeneration happens because part of the halo area becomes of infinite small width. Table 2 summarizes the properties of degenerated halos.

Every type of halo in Tables 1 and 2 has in principle a different intensity distribution and polarization characteristic, so these characteristics must be calculated separately. In Sections 6 and 7 this is done explicitly for the most prominent halos: the circumzenithal arc, the parhelia, the tangent arcs, and the 22° halo.

#### 4. HALO FORMULAS AND CALCULATION PROCEDURE

If the orientation  $(i, h, q)$  of a given ice crystal is fixed, the polar coordinates of the refracted light are known according to the following set of formulas:

$$D = i + i' - A, \quad (1)$$

$$\sin i = n' \sin r, \quad \sin i' = n' \sin r',$$

$$n' = \left( \frac{n^2 - \sin^2 h}{\cos^2 h} \right)^{1/2}, \quad (2)$$

$$\sin \theta/2 = \sin D/2 \cos h, \quad (3)$$

and

$$\phi = q + \phi', \quad (4)$$

where

$$\cos \phi' = \frac{\cos h \sin D}{\sin \theta} \quad (5)$$

(see Ref. 10, p. 109). (See Appendix A for the definition of the angles.) In the case of minimum deviation,  $i = i' = i_m$  and  $r = r' = r_m$ . Since  $2r_m = A$ , we have from Eq. (1) the relation  $2i_m = D_m + A$ . Then Eq. (2) reduces to the well-known formula

$$\sin \frac{D_m + A}{2} = n' \sin \frac{A}{2}. \quad (6)$$

The halo angle  $\theta_h \equiv D_h$  can be found from Eq. (6) for  $h = 0$ , which replaces  $n'$  with  $n$ . Note that  $\theta = \theta(i, h)$  and  $\phi = \phi(i, h, q)$ . So the scattering angle depends on only two of the crystal coordinates. We call the functions  $\theta = \theta(i, h)$  and  $\phi = \phi(i, h, q)$  the *deflection functions* for ice crystals.

Specifying the geometry of a crystal and the degree of freedom in a set of them, formulas (1)–(6), permits the calculation of the intensity distribution, shapes, and polarization of the resulting halos if one also takes into account the Fresnel polarization and the birefringence of ice. However, such a

calculation is complicated and should be performed numerically. To simplify this procedure, we make five assumptions:

(1) The variation of the Fresnel coefficients with  $i$  and  $h$  is neglected.

(2) Geometric obstructions in the crystals are neglected.

(3) The number of ice crystals is assumed to be equal along every line of sight.

(4) Only ray optics is taken into consideration.

(5) A preferential orientation is assumed to be realized completely for all crystals [see Section 8 for the effect of a departure of this (e.g., vibrating crystals)].

Under these assumptions, the intensity at (solid) angle  $d\omega$  is proportional only to the number of crystals  $dN$  that give rise to scattering in this angle. Thus

$$I \propto dN/d\omega. \quad (7)$$

In Section 5,  $\theta(i, h)$  and  $\phi(i, h, q)$  are developed in truncated Taylor expansions to make possible a formulation of expression (7) in simple analytical expressions.

#### 5. SIMPLIFIED HALO FORMULAS

From Eqs. (1)–(5) we see that the polar coordinates of light that is deflected by two refractions in an ice crystal are functions of the crystal orientations:

$$\begin{aligned} \theta &= \theta(i, h), & D &= D(i, h), \\ \phi &= \phi(i, h, q) \equiv q + \phi'(i, h). \end{aligned} \quad (8)$$

We would like to know the behavior of these functions near  $i = i_m$  and  $h = 0$ . Since  $i_m = i_h$  at  $h = 0$ , it is convenient to replace  $i$  with a new coordinate,

$$\alpha = i - i_h, \quad (9)$$

so that the functions are changed into  $\theta(\alpha, h)$ ,  $D(\alpha, h)$ , and  $\phi(\alpha, h, q)$ . The halo angle is  $\theta_h = \theta(0, 0) = D(0, 0)$ , and the angle of minimum deviation is  $D_m = D(i_m - i_h, h)$ . We now calculate the Taylor expansions for  $D$ ,  $\theta$ , and  $\phi$ .

For the deviation function  $D(\alpha, h)$ , one obviously has

$$\left( \frac{\partial D(\alpha, h)}{\partial \alpha} \right)_{\alpha=0}^{h=0} = 0. \quad (10)$$

The other first derivative can be found from Ref. 11, Eq. (7–8)

$$\frac{\partial D(\alpha, h)}{\partial h} = \frac{\partial D}{\partial n'} \frac{dn'}{dh} = \frac{\sin A}{\cos r \cos i'} \frac{(n^2 - 1) \sin h}{n' \cos^3 h}, \quad (11)$$

which is zero at  $h = 0$ .

From Eq. (11), one finds also that  $\partial^2 D / \partial \alpha \partial h$  is zero at  $(\alpha, h) = (0, 0)$ , so that the Taylor expansion to be used becomes

$$\begin{aligned} D(\alpha, h) &\simeq D(0, 0) + 1/2 \left( \frac{\partial^2 D(\alpha, 0)}{\partial \alpha^2} \right)_{\alpha=0} \alpha^2 \\ &\quad + 1/2 \left( \frac{\partial^2 D(0, h)}{\partial h^2} \right)_{h=0} h^2 \quad (12) \\ &\equiv D(0, 0) + C_1 \alpha^2 + C_2 h^2. \end{aligned} \quad (13)$$

For

$$C_1 = 1/2 \left( \frac{\partial^2 D}{\partial \alpha^2} \right)_{\alpha=0} \equiv 1/2 \left( \frac{\partial^2 D}{\partial i^2} \right)_{i=i_h},$$

one finds that

$$C_1 = \frac{n \cos^2 r_h \sin i_h - \cos^2 i_h \sin r_h}{n \cos i_h \cos^2 r_h} \equiv \frac{1}{\cos^2 r_h} \left( 1 - \frac{1}{n^2} \right) \tan i_h. \tag{14}$$

The first expression for Eq. (14) can be found in Ref. 9, p. 503, if one takes into account that  $i_m = i_h$  at  $h = 0$ ; the last expression follows from some reductions made using Snell's law.

From Eq. (11), one finds, using  $A = 2r_h$  and Snell's law again, that

$$\begin{aligned} \left( \frac{\partial^2 D}{\partial h^2} \right)_{\alpha=0} &= \left( \frac{d^2 n'}{dh^2} \right)_{h=0} \left( \frac{\sin A}{\cos i' \cos r} \right)_{\alpha=0} \\ &= \frac{n^2 - 1}{n} \frac{\sin 2r_h}{\cos i_h \cos r_h} \\ &= \frac{n^2 - 1}{n} \frac{2 \sin r_h}{\cos i_h} = 2 \frac{n^2 - 1}{n^2} \tan i_h, \end{aligned} \tag{15}$$

so that the second constant becomes

$$C_2 = \left( 1 - \frac{1}{n^2} \right) \tan i_h. \tag{16}$$

This reduces  $D(\alpha, h)$  for small  $\alpha$  and  $h$  to the desired relation

$$D(\alpha, h) = D(0, 0) + C_1 \alpha^2 + C_2 h^2. \tag{13'}$$

This approximation can be used to calculate the deviation in an accurate way up to at least  $D = 32^\circ$  for the  $22^\circ$  halo group. Of course, if  $D$ ,  $\alpha$ , and  $h$  are expressed in degrees, the parameters  $D(\alpha, h)$  and  $D(0, 0)$  should be multiplied by  $180/\pi$  in Eq. (13').

The relation between  $D(\alpha, h)$  and the first deflection function  $\theta(\alpha, h)$  is given by

$$\sin[\theta(\alpha, h)/2] = \sin[D(\alpha, h)/2] \cos h, \tag{3'}$$

which implies that  $\partial^2 \theta \alpha, 0/\partial \alpha^2 = \partial^2 D \alpha, 0/\partial \alpha^2$  and that  $[\partial \theta \alpha, h/\partial h]_{h=0} = 0$ . From Eq. (3') one finds also for the second derivative that

$$\left( \frac{\partial^2 \theta(0, h)}{\partial h^2} \right)_{h=0} = -2 \tan[\theta(0, 0)/2] + \left( \frac{\partial^2 D(0, h)}{\partial h^2} \right)_{h=0}. \tag{17}$$

So  $\theta(\alpha, h)$  reduces with the same expansion as expression (12) to

$$\theta(\alpha, h) = \theta(0, 0) + C_1 \alpha^2 + C_3 h^2, \tag{18}$$

with

$$C_3 = \left( 1 - \frac{1}{n^2} \right) \tan i_h - \tan[\theta(0, 0)/2] \equiv C_2 - \tan[\theta(0, 0)/2]. \tag{19}$$

This formula has an accuracy of  $0.5^\circ$  or better compared with the exact expressions (1)-(5) at  $\theta = 27^\circ$  for the  $22^\circ$  halo group.

For the nondegenerate one-dimensional halos,  $\alpha = \alpha(h)$ , which urges a further evaluation of Eq. (18) in these cases. For a horizontally oriented entry face, as in the case for the circumzenithal arc, the relation between  $\alpha$  and  $h$  is given in Ref. 10, p. 119:

$$\cos(\alpha + i_h) = \sin \Sigma / \cos h. \tag{20}$$

If the entry face is sloped, as is the case for the circumhorizontal arc and for several types of Parry arcs, the angle of inclination of the entry face should be added to  $i_h$  in Eq. (20).

We define  $\alpha = \alpha_0$  for  $h = 0$ . Expanding Eq. (20) in a Taylor expansion again, one gets

$$\alpha \simeq \alpha_0 - \frac{\sin \Sigma}{2 \sin(\alpha_0 + i_h)} h^2, \tag{21}$$

in which  $\alpha_0 + i_h = 90^\circ - \Sigma$  in the case of the circumzenithal arc. Substituting expression (21) into Eq. (18) and neglecting the  $h^4$  terms results in

$$\begin{aligned} \theta(h) &= \theta(0, 0) + C_1 \alpha_0^2 + \left[ C_3 - \frac{\alpha_0 \sin \Sigma}{\sin(\alpha_0 + i_h)} \right] h^2 \\ &\equiv \theta(0, 0) + C_1 \alpha_0^2 + C'_3 h^2. \end{aligned} \tag{22}$$

For  $\alpha_0 = 0$ ,  $C'_3 = C_3$ , but, for another  $\alpha_0$ ,  $C'_3$  may differ considerably from  $C_3$ . Since  $\theta(\alpha_0, 0) = \theta(0, 0) + C_1 \alpha_0^2$  represents the scattering angle in the solar vertical, it makes sense to change Eq. (22) to

$$\theta(h) = \theta(\alpha_0, 0) + C'_3 h^2, \tag{23}$$

which is the ultimate expression for the first deflection function for the nondegenerated one-dimensional halos, including the circumzenithal arc.

The expansion of the second deflection function  $\phi(\alpha, h, q) = q + \phi'(\alpha, h)$  is simpler, since here the first derivatives are generally nonzero. One has for  $\phi'(h, q)$  the exact expression

$$\cos \phi'(\alpha, h) = \frac{\cos h \sin D(\alpha, h)}{\sin \theta(\alpha, h)}, \tag{5'}$$

which reduces for small  $\phi'$  to

$$\begin{aligned} 1 - \frac{\phi'^2(\alpha, h)}{2} &\simeq \left( 1 - \frac{h^2}{2} \right) \left[ \frac{\sin D(0, 0) + \cos D(0, 0) dD}{\sin \theta(0, 0) + \cos \theta(0, 0) d\theta} \right] \\ &\simeq \left( 1 - \frac{h^2}{2} \right) [1 + \cotan \theta(0, 0) d\theta] \\ &\quad \times [1 - \cotan \theta(0, 0) d\theta]. \end{aligned} \tag{24}$$

Inserting  $dD = C_1 \alpha^2 + C_2 h^2$  and  $d\theta = C_1 \alpha^2 + C_3 h^2$  leads to

$$1 - \frac{\phi'^2(\alpha, h)}{2} \simeq 1 - [1/2 - (C_2 - C_3) \cotan \theta(0, 0)] h^2, \tag{25}$$

which implies that  $\phi'(\alpha, h)$  is in first approximation independent of  $\alpha$ .

Using Eq. (19) for the relation between  $C_2$  and  $C_3$ , one gets finally, for the behavior of  $\phi'$  for small  $\alpha$  and  $h$ ,

$$\phi'(h) = \tan[\theta(0, 0)/2] h, \tag{26}$$

so that the second deflection function becomes

$$\phi(h, q) = q + \tan[\theta(0, 0)/2]h. \quad (27)$$

If the axial vector  $\hat{P}$  is horizontal (which is the case for the tangent arcs), we find along similar lines, starting from Ref. 10, p. 110, that

$$\phi(h) = \{\tan[\theta(0, 0)/2] \pm \tan \Sigma\}h \equiv C_4 h, \quad (28)$$

where the plus refers to the upper arc and the minus to the lower one. For the sake of simplicity, we chose in Eq. (28)  $\phi = 0$  for both the upper and the lower arcs in the solar vertical ( $h = 0$ ). Note that for the lower arc,  $C_4 = 0$  at a solar elevation  $\Sigma = 1/2 \theta(0, 0)$ , indicating one of the rare singularities of this arc at the subsolar point, which results in the curious shape of this arc in this region.<sup>11,12</sup>

For the one-dimensional circumzenithal, circumhorizontal, or Parry arcs, one finds in the same way a slightly different expression for the second deflection function:

$$\phi(h) = \{\tan[\theta(\alpha_0, 0)/2] \pm \tan \Sigma\}h \equiv C'_4 h, \quad (29)$$

in which the plus again refers to the upper arcs.

## 6. INTENSITY DISTRIBUTIONS AND SHAPES OF HALOS

Formulas (13), (18), (23), and (27)–(29) permit the calculation of the intensity distributions of all types of refraction halos. Under the assumption in Section 4, these intensity distributions are given by

$$I(\theta) = dN/d\omega, \quad (7')$$

where  $I(\theta)$  is in normalized units and where  $N$  represents the number of crystals giving rise to scattering in a (solid) angle element  $d\omega$  at position  $(\theta, \phi)$ . In general,  $d\omega = \sin \theta d\theta d\phi$ , but for one-dimensional halos  $d\omega$  is also one dimensional. Since  $N$  also differs for all types of halo, formula (7') had to be worked out separately for these cases.

When the intensity distribution  $I(\theta)$  is known for a point source, it is possible to obtain a more realistic intensity distribution  $\bar{I}(\theta)$  by integrating  $I(\theta)$  over the solar disk. Basically, this is done in the solar vertical ( $\phi = 0$ ), since it can be shown that there the shape of the nondegenerate halo or the halo caustic under consideration is almost a straight line on the scale of the solar disk, being perpendicular to the solar vertical. Then the integration is found by

$$\bar{I}(\theta) = \frac{2}{\pi s^2} \int_{\max(\theta_h, \theta-s)}^{\theta+s} I(y)g(y-\theta)dy, \quad (30)$$

where  $g(x) = (s^2 - x^2)^{1/2}$  represents the shape of the sun and  $s = 0.25^\circ$  is the semidiameter of the solar disk. Because of the factor  $2/(\pi s^2)$ ,  $I(\theta)$  and  $\bar{I}(\theta)$  can be expressed in the same units.

In the case of the parhelia, which is basically a radially directed line, the integration has to be performed along a line segment of the sun, so that Eq. (30) reduces to

$$\bar{I}(\theta) = \frac{1}{2s} \int_{\max(\theta_h, \theta-s)}^{\theta+s} I(y)dy. \quad (31)$$

We now discuss the intensity distributions of the circumzenithal arc, the parhelia, the tangent arcs, and the 22° halo.

### Circumzenithal Arc

For a nondegenerate one-dimensional halo, there exist two relations between  $i$ ,  $h$ , and  $q$ . Specifying one of these angles is therefore sufficient to fix the orientation of generating crystals in space. We choose  $h$  for this. Since the halo is an infinite thin line  $l$  in the firmament, Eq. (7) becomes

$$I(\theta) = dh/dl. \quad (32)$$

If Eq. (23) is substituted into Eq. (29), the shape of the line is given by

$$\theta - \theta(\alpha_0, 0) = \frac{C'_3}{C'^2_4} \phi^2 \equiv C'_5 \phi^2, \quad (33)$$

in which for  $C_4$  the plus must be applied. Formula (33) shows that the departure of the circumzenithal arc from a circle around the sun with radius  $\theta(\alpha_0, 0)$  is a smooth parabola. This is indeed the shape of the circumzenithal arc near the solar vertical. The length of a line segment of it is given by

$$\begin{aligned} dl &= \left[ \sin^2 \theta + \left( \frac{d\theta}{d\phi} \right)^2 \right]^{1/2} d\phi \simeq \left[ \sin^2 \theta(\alpha_0, 0) + \left( \frac{d\theta}{d\phi} \right)^2 \right]^{1/2} d\phi \\ &= [\sin^2 \theta(\alpha_0, 0) + 4C'^2_5 \phi^2]^{1/2} d\phi, \end{aligned} \quad (34)$$

so that the right-hand term of Eq. (32) becomes, by applying Eq. (29) again,

$$\frac{dh}{dl} = \frac{dh}{d\phi} \frac{d\phi}{dl} = \frac{1}{C'_4} \frac{1}{[\sin^2 \theta(\alpha_0, 0) + 4C'^2_5 \phi^2]^{1/2}}. \quad (35)$$

Taking into account the infinite small width of the halo, this leads to

$$I(\theta) = \frac{\delta[\theta - \theta(\alpha_0, 0) - C'_5 \phi^2]}{C'_4 [\sin^2 \theta(\alpha_0, 0) + 4C'^2_5 \phi^2]^{1/2}}, \quad (36)$$

where  $\delta(x)$  is the Dirac delta function<sup>13</sup> and the constants depend only on the solar elevation. On the solar vertical, this reduces to

$$I(\theta) = \delta[\theta - \theta(\alpha_0, 0)], \quad (37)$$

where  $I(\theta)$  is in normalized units. The intensity distribution  $\bar{I}(\theta)$  for a finite sun in the same units can be found from Eqs. (30) and (37):

$$\begin{aligned} \bar{I}(\theta) &= \frac{2}{\pi s^2} \int \delta[y - \theta(\alpha_0, 0)] [s^2 - (y - \theta)^2]^{1/2} dy \\ &= \frac{2}{\pi s^2} [s^2 - [\theta - \theta(\alpha_0, 0)]^2]^{1/2}. \end{aligned} \quad (38)$$

This intensity distribution is essentially an ellipse centered at  $\theta = \theta(\alpha, 0)$  and is shown in Fig. 2.

### Parhelia

This degenerate one-dimensional halo represents a mapping of  $\alpha$  in  $D$ . The degeneration occurs because  $h = \Sigma$  for any  $\alpha$ , so that the orientation of a crystal can be specified only by  $\alpha$  but never by  $h$  or  $q$ . For parhelia Eq. (7) is represented by

$$I = d\alpha/dD. \quad (39)$$

For simplicity, we restrict ourselves to  $\Sigma = 0$ ; for other solar elevations essentially the same formulas can be obtained since  $D(\alpha, h) - D(0, 0) = C_1 \alpha^2 + C_2 h^2$  [Eq. (13)] reduces to  $D(\alpha, \Sigma) - D(0, 0) - C_2 \Sigma^2 = D(\alpha, 0) - D(0, \Sigma) = C_1 \alpha^2$ . Of course,

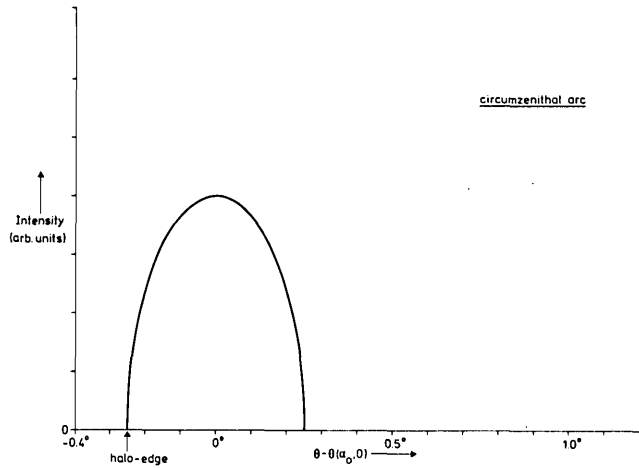


Fig. 2. Intensity distribution of the circumzenithal arc as a function of scattering angle  $\theta$  in the solar vertical for a finite sun.  $\theta(\alpha_0, 0)$  denotes the position of this halo for a point-shaped sun.

for  $\Sigma \neq 0$  the intensity distribution of the parhelia should be measured along the solar almucanter instead of along  $\phi = \pm 90^\circ$ .

For  $\Sigma = 0$ , one has  $h = 0$  and  $D(\alpha, 0) = \theta(\alpha, 0)$ , with  $\theta(\alpha, 0) - \theta(0, 0) = C_1\alpha^2$ . Inserting this into Eq. (39), one finds, replacing  $\theta(0, 0)$  with  $\theta_h$ , that

$$I(\theta) = \frac{1}{(\theta - \theta_h)^{1/2}}, \tag{40}$$

where  $I(\theta)$  is again in normalized units. The integration over the solar disk according to Eq. (31) results in

$$\begin{aligned} \bar{I}(\theta) &= \frac{1}{s} (\theta - \theta_h + s)^{1/2}, & -s < \theta - \theta_h < s, \\ \bar{I}(\theta) &= \frac{1}{s} [(\theta - \theta_h + s)^{1/2} - (\theta - \theta_h - s)^{1/2}], & \theta - \theta_h > s, \end{aligned} \tag{41}$$

$\bar{I}(\theta)$  and  $I(\theta)$  being in the same units. The resulting graphs are shown in Fig. 3.

**Tangent Arcs**

For two-dimensional halos,  $dN$  can be closely approximated by  $dN \propto \alpha d\alpha dh$  for the relevant part of the generating set of crystals. Furthermore,  $d\omega = \sin \theta d\theta d\phi \approx \sin \theta_h d\theta d\phi$  near  $\theta = \theta_h$ , which is our range of interest. If one takes  $\sin \theta_h$  as a constant, Eq. (7) becomes

$$I(\theta) = \frac{dh d\alpha}{d\phi d\theta} = \frac{1}{C_4} \frac{d\alpha}{d\theta} \tag{42}$$

since  $\alpha$  does not depend on  $h$ . Combining Eqs. (18) and (28), one gets

$$\theta(\alpha, h) = \theta_h + C_1\alpha^2 + \frac{C_3}{C_4^2} \phi^2 \equiv \theta_h + C_1\alpha^2 + C_5\phi^2. \tag{43}$$

If Eq. (43) is inserted into Eq. (42) and the units are changed so that  $C_1 = C_4 = 1$ , the intensity distribution becomes

$$I(\theta) = \frac{1}{(\theta - \theta_h - C_5\phi^2)^{1/2}}, \tag{44}$$

which is at  $\phi = 0$  ( $h = 0$ ) identical to the intensity distribution of a parhelia [Eq. (40)].

The shape of the caustic of the tangent arcs near  $\phi = 0$  can

be found by making the denominator of Eq. (44) zero, which results in a parabola, as was also the case for the circumzenithal arc:

$$\theta - \theta_h = C_5\phi^2 \equiv \frac{C_3}{C_4^2} \phi^2. \tag{45}$$

Since  $C_4 = [\tan(\theta_h/2) \pm \tan \Sigma]$  [Eq. (28)] and the minus stands for the lower-tangent arc, the expression indicates also that, for every refracting angle  $A$ , the parabola of the lower-tangent arc is sharper than the one for the upper-tangent arc. Of course, for  $C_4 = 0$  the expression breaks down, but away from this point the parabola is sufficiently smooth to calculate  $\bar{I}(\theta)$  from Eqs. (30) and (44) for  $\phi = 0$ , resulting in

$$\bar{I}(\theta) = \frac{2}{\pi s^2} \int_{\max(\theta_h, \theta-s)}^{\theta+s} \left[ \frac{s^2 - (y - \theta)^2}{y - \theta_h} \right]^{1/2} dy. \tag{46}$$

This integral cannot be expressed in elementary functions and should be solved numerically. However, the result is close to the one for parhelia, as can be seen in Fig. 4.

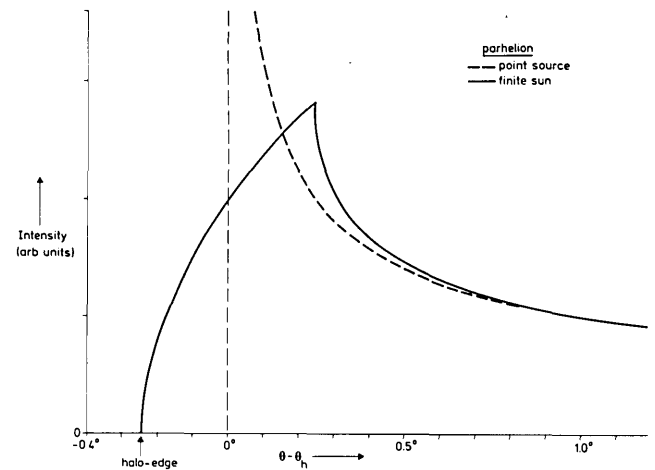


Fig. 3. Intensity distribution of a parhelia as a function of scattering angle  $\theta$  for a point source and for a finite sun.  $\theta_h$  denotes the halo angle. The figure refers to zero solar elevation, but for another solar elevation the intensity distribution is the same.

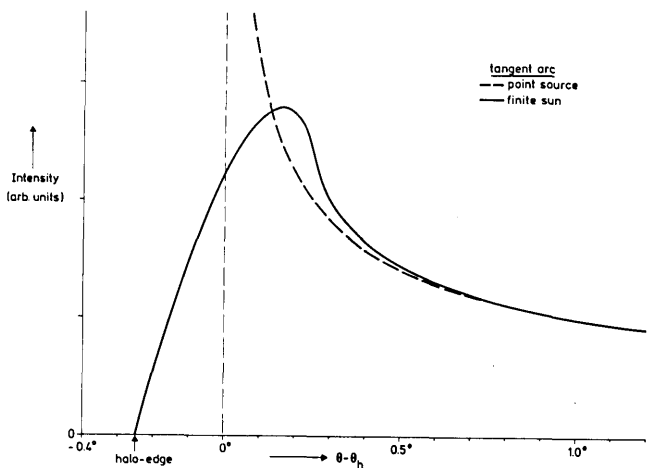


Fig. 4. Intensity distribution of a tangent arc as a function of scattering angle  $\theta$  in the solar vertical for a point source and for a finite sun.  $\theta_h$  denotes the halo angle.

Since the main purpose of this paper is to find the polarization of prominent refraction halos, we will not discuss the

rather complicated calculation of the lower-tangent arc near the subsolar point (or of other rarely observed phenomena) in detail. We only mention the fact that in our expansions the shape of a lower-tangent arc for  $2\Sigma = \theta_h$  is given by

$$(\theta - \theta_h) \propto \phi^{2/3}, \quad (47)$$

which thus represents a close description of Szlavik's famous picture of the lower arc at a solar elevation of about  $11^\circ$  (Ref. 10, plate IV.2).

**22° Halo**

Surprisingly, the calculation of the three-dimensional halo is quite simple. We first treat the second deflection function  $\phi(h, q)$  and choose a fixed  $\phi$ , say,  $\phi = 0$ . Since random orientation is present, all values for  $\alpha, h$ , and  $q$  are realized in the cloud of ice crystals, but formula (27) shows that only the subset  $\{\alpha, h, q\} = \{\alpha, h, -\tan[\theta(0, 0)/2]h\}$  contributes to scattering in  $\phi = 0$ . So, if one chooses a fixed  $h = h_0$ , there is always one and only one element  $q_0$  present in the set of  $\{q\}$  that gives rise to scattering in a fixed  $\phi = \phi_0$ . Since Eq. (27) indicates a linear relationship between  $h_0$  and  $q_0$ , this property means that, for deriving the intensity distribution of halos generated by randomly oriented crystals along a fixed  $\phi = \phi_0$ , we have to consider only the set  $\{\alpha, h\}$ , treating the second deflection function  $\phi(q, h) = \phi_0$  as a constant. Therefore, for the 22° halo, the first deflection function

$$\theta(\alpha, h) = \theta_h + C_1\alpha^2 + C_3h^2 \quad (18')$$

is the only one that has to be evaluated. This function represents a paraboloid. The number of particles  $N$  that gives rise to scattering at angles below a fixed  $\theta$  can be represented by the area of an ellipse in the  $(\alpha, h)$  plane, which contains all pairs  $(\alpha, h)$  with this property. This is the area size of an ellipse [Eq. (18')] for  $\theta(\alpha, h) = \theta$ . Calculating from Eq. (18') the length of the two axes of the ellipse, one finds that

$$N \propto \pi \frac{\theta - \theta_h}{(C_1 C_3)^{1/2}} \propto \theta - \theta_h \quad \text{if } \theta - \theta_h > 0, \\ N = 0 \quad \text{if } \theta - \theta_h < 0. \quad (48)$$

With  $d\omega = 2\pi \sin \theta d\theta$  and  $\theta \simeq \theta_h = \text{constant}$ , the relevant part of Eq. (7) along every curve  $\phi = \text{constant}$  becomes

$$I(\theta) = dN/d\theta, \quad (49)$$

so that the intensity distribution in normalized units is given by

$$I(\theta) = H(\theta - \theta_h), \quad (50)$$

where  $H(x)$  is the Heaviside step function,<sup>13</sup>

$$H(x) = 1, \quad x > 0, \\ H(x) = 0, \quad x < 0. \quad (51)$$

Integrating over the solar disk again, one obtains from Eq. (30)

$$\bar{I}(\theta) = 1/2 + \frac{1}{\pi} \arcsin \frac{\theta - \theta_h}{s} + \frac{\theta - \theta_h}{\pi s^2} [s^2 - (\theta - \theta_h)^2]^{1/2},$$

$$\bar{I}(\theta) = 1, \quad \theta - \theta_h > s.$$

The resulting plots are given in Fig. 5. It should be noted that Eq. (50) can also be obtained by integrating the intensity

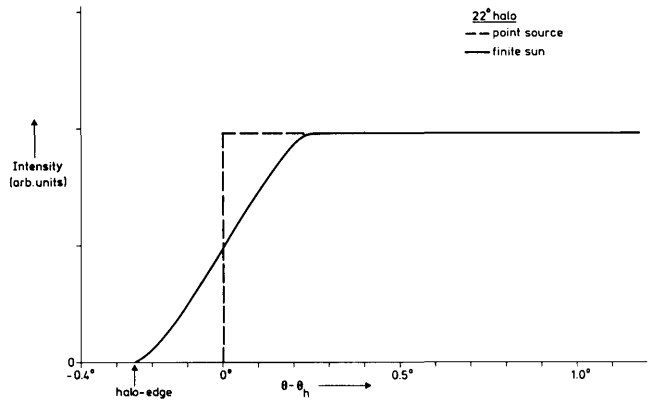


Fig. 5. Intensity distribution of the 22° halo as a function of scattering angle  $\theta$  for a point source and for a finite sun.  $\theta_h$  denotes the halo angle.

distribution of the tangent arc [Eq. (44)] along  $\phi$  since the 22° halo can be considered the superposition of a tangent arc that rotates around the sun.<sup>11</sup>

**7. POLARIZATION DISTRIBUTIONS OF HALOS**

The two contributions to polarization of refraction halos are Fresnel refraction and birefringence. We treat them both in this section, but first we give some general remarks and introduce some new definitions.

Since birefringence leads to different halo angles for the two directions of polarization, it is not useful to express the polarization distributions in  $\theta - \theta_h$  anymore. Therefore we change the scattering coordinate into  $\theta - \theta_{\text{edge}}$ , where  $\theta_{\text{edge}} = \theta_h - s$  for the polarized component closest to the sun.

Because polarization by birefringence results from a shift of two polarized halos, it is also not convenient to describe the polarization distributions in terms of the degree of polarization  $P$ . We choose here to express them as  $I_1 - I_2 = I_{\text{pol}}$ , which represents the quantity of polarized light. From this the degree of polarization  $P$  may be calculated by

$$P = \frac{-I_{\text{pol}}}{I_1 + I_2 + I_B}, \quad (53)$$

where  $I_B$  is the intensity of a background. Of course, near  $\theta_{\text{edge}}$ ,  $P = 100\%$  or  $P = -100\%$  for  $I_B = 0$ , since either  $I_1$  or  $I_2$  is zero because of the shift between the polarized halos. If  $P < 0$ , the electrical vector of the polarized light is in the plane of scattering. In that case,  $I_{\text{pol}} > 0$ .

**Fresnel Refraction**

In this approach we consider the Fresnel-refraction contribution to the polarization for a given halo to be constant along  $\theta$ . In the angular region of interest to us, this is a good approximation. So we can restrict ourselves to calculating the relative intensity of  $I_1$  and  $I_2$  at the halo angle  $\theta_h \equiv \theta(0, 0)$ ,

$$-s < \theta - \theta_h < s, \quad (52)$$

which is given by the ratio of the Fresnel coefficients for two refractions:

$$I_1/I_2 = \left[ 1 - \frac{\tan^2(i_h - r_h)}{\tan^2(i_h + r_h)} \right]^2 \left[ 1 - \frac{\sin^2(i_h - r_h)}{\sin^2(i_h + r_h)} \right]^{-2}. \quad (54)$$

After some goniometric manipulations, and keeping in mind that  $i_h - r_h = \theta_h/2$ , this reduces to

$$I_1/I_2 = \cos^{-4}(\theta_h/2). \quad (55)$$

For the 22° halo group  $I_1/I_2 = 1.077$ , and for the 46° halo group  $I_1/I_2 = 1.39$ , which corresponds to degrees of polarization of 3.7% and 16%, respectively. It should be noted that the approximation  $I_1/I_2(\theta) \approx I_1/I_2(\theta_h)$  that we apply here is better for the one- and two-dimensional halos than for the three-dimensional ones since for the latter a skew transfer of light through a crystal ( $h \neq 0$ ) causes a relatively quick decrease of  $\|I_1 - I_2\|$  as a function scattering of angle.

**Birefringence**

The transfer of light through an anisotropic prism has been calculated for the most general case by White.<sup>7</sup> Of course, for the ordinary refracted rays (subject to an index of refraction

$n_o$ ), the halo formulas [Eqs. (1)–(6)] remain unchanged, but, for the extraordinary refracted rays (index of refraction  $n_e$ ), the resulting formulas are rather complicated. However, if the birefringence  $\delta n = n_e - n_o$  is small, as in the case of ice, White's formulas can be simplified significantly. It can be proved that in that case the halo formulas, and therefore also our formalism, can also be applied for the extraordinary rays if one replaces in all formulas the index of refraction  $n$  with an effective index of refraction  $n_{\text{eff}}$ , which is given by

$$n_{\text{eff}} = n_o + \sin^2 \gamma (n_e - n_o) \equiv n_o + \sin^2 \gamma \delta n. \quad (56)$$

Here  $\gamma$  is the angle between the light path in the crystal, which gives rise to scattering at the halo angle ( $h = \alpha = 0$ ), and the optical axis of the crystal. For the 22° halo group,  $\gamma = 90^\circ$  so that  $n_{\text{eff}} = n_e$ , but for the 46° halo group  $\gamma = 45^\circ$ , and thus  $n_{\text{eff}} = 1/2 n_o + 1/2 n_e$ .

The angular shift in the intensity distribution of the polarized components of a halo can be found from differentiating the minimum-deviation formula for  $h = 0$ :

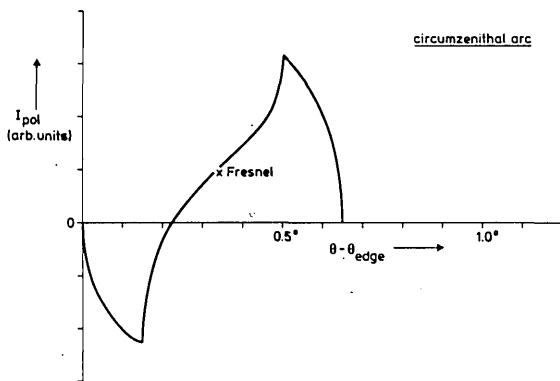


Fig. 6. Quantity of polarized light  $I_{\text{pol}} = I_1 - I_2$  for the circumzenithal arc as a function of scattering angle  $\theta$  in the solar vertical for a finite sun.  $\theta_{\text{edge}}$  denotes the inner edge of the halo. Near  $\theta_{\text{edge}}$  only ordinary refracted rays contribute to the light of the halo. For comparison, at the intensity maximum of the halo,  $I_{\text{pol}}$  is also given for Fresnel refraction alone. If  $I_{\text{pol}} > 0$ , the polarization is in the plane of scattering.

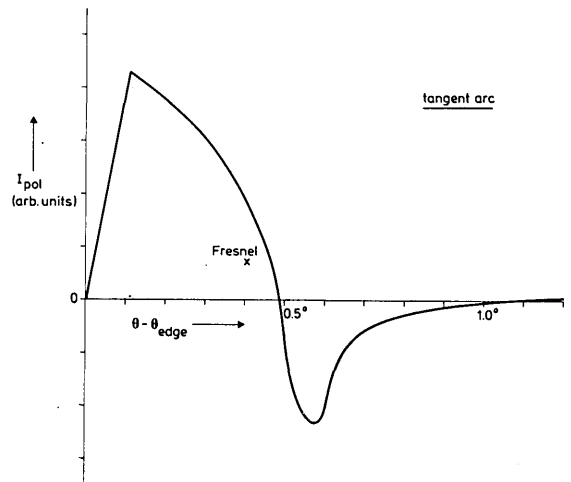


Fig. 8. Quantity of polarized light  $I_{\text{pol}} = I_1 - I_2$  for a tangent arc as a function of scattering angle  $\theta$  in the solar vertical for a finite sun.  $\theta_{\text{edge}}$  denotes the inner edge of the halo. Near  $\theta_{\text{edge}}$  only ordinary refracted rays contribute to the light of the halo. For comparison, at the intensity maximum of the halo,  $I_{\text{pol}}$  is also given for Fresnel refraction alone. If  $I_{\text{pol}} > 0$ , the polarization is in the plane of scattering.

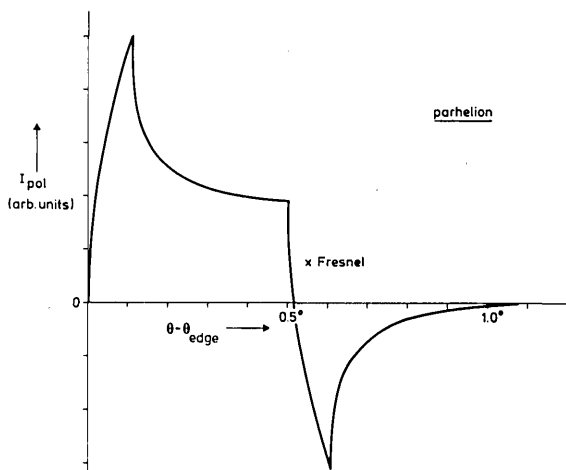


Fig. 7. Quantity of polarized light  $I_{\text{pol}} = I_1 - I_2$  for the parhelson as a function of scattering angle  $\theta$  for a finite sun.  $\theta_{\text{edge}}$  denotes the inner edge of the halo. Near  $\theta_{\text{edge}}$  only ordinary refracted rays contribute to the light of the halo. For comparison, at the intensity maximum of the halo,  $I_{\text{pol}}$  is also given for Fresnel refraction alone. If  $I_{\text{pol}} > 0$ , the polarization is in the plane of scattering.

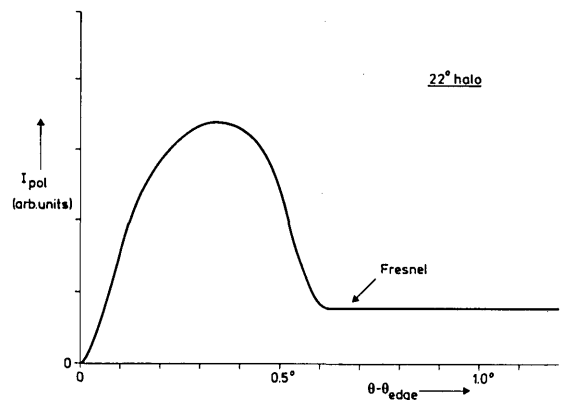


Fig. 9. Quantity of polarized light  $I_{\text{pol}} = I_1 - I_2$  for the 22° halo as a function of scattering angle  $\theta$  for a finite sun.  $\theta_{\text{edge}}$  denotes the inner edge of the halo. Near  $\theta_{\text{edge}}$ , only ordinary refracted rays contribute to the light of the halo. For  $\theta - \theta_{\text{edge}} > s + 0.11^\circ$ , only Fresnel refraction contributes to the polarization of the 22° halo. For any  $\theta$ , the polarization is in the plane of scattering.

$$\cos \frac{\theta_h + A}{2} d\theta_h = \sin(A/2)(n_{\text{eff}} - n_o). \quad (57)$$

The birefringence of ice  $\delta n = 0.0014$  (Ref. 14) and is almost independent of the wavelength for the visible range. This leads to a difference in the halo angle  $\Delta\theta_h$  for the polarized components of  $0.11^\circ$  for the  $22^\circ$  halo group and to  $0.15^\circ$  for the  $46^\circ$  halo group.

Since  $n_o$  is smaller than  $n_e$ , the halo that is due to ordinary refraction is always closest to the sun. The direction of its polarization is perpendicular to the optical axis of the crystals. In the case of the  $22^\circ$  halo group, the optical axes of the contributing crystals are in principle perpendicularly oriented with respect to any line halo sun. This means that the polarization of the inner edge of the halo (where only the ordinary refracted rays are present) is in the plane of scattering. For the  $46^\circ$  halo group the situation is reversed. So in this case the polarization of its inner edge is perpendicular to the component that is due to Fresnel refraction.

The quantity of polarized light for a finite sun becomes

$$I_{\text{pol}} = \bar{I}(\theta - \theta_{\text{edge}}) - \cos^4 11^\circ \bar{I}(\theta - \theta_{\text{edge}} - 0.11^\circ),$$

$$I_{\text{pol}} = \bar{I}(\theta - \theta_{\text{edge}} - 0.15^\circ) - \cos^4 23^\circ \bar{I}(\theta - \theta_{\text{edge}}) \quad (58)$$

for the  $22^\circ$  and the  $46^\circ$  halo group, respectively. For the four typical halos, these polarization distributions are plotted near the halo edges in Figs. 6–9. For comparison, at the halo maximum ( $\theta - \theta_{\text{edge}} \simeq s$  and  $\theta - \theta_{\text{edge}} \simeq 2s$  for the circumzenithal arc and the  $22^\circ$  halo group, respectively),  $I_{\text{pol}}$  is given also for the case in which only Fresnel refraction should contribute to the polarization. This should result in an almost constant degree of polarization of about 4% for the  $22^\circ$  halo group and of 16% for the  $46^\circ$  halo group over the whole angular range visualized in the figures. These data permit the calculation of the degree of polarization  $P$  from Eq. (53) as a function of scattering angle if some background intensity  $I_B$  is present.

## 8. DISCUSSION

### Intensity Distributions and Color Distributions

In the previous sections, it was shown that there are dramatic differences in the intensity distributions of halos of various classes. For a point source the circumzenithal arc is a curve of infinite small width, the parhelion is a curve with a caustic, the tangent arc is an area with a similar caustic toward the sun, and the intensity distribution of the  $22^\circ$  halo can be represented by a step function. This means, e.g., that the circumscribed halo even at high solar elevations can be distinguished from the  $22^\circ$  halo by its intensity distribution and even more clearly, as we see below, by its color distributions. The above-mentioned properties of the various intensity distributions can be seen clearly in the plots of Greenler,<sup>5</sup> in which, e.g., his points of the parhelia are distinctly more concentrated near the halo edge than the points for the  $22^\circ$  halo. Moreover, in his plate 3-3, he shows a parhelion for vibrating crystals, which means that he added two additional degrees of freedom to the set of generating crystals contributing to scattering near the halo angle. Indeed, the resulting plot resembles closely the one of the  $22^\circ$  halo.<sup>5</sup> On the other hand, Greenler's plots of the  $22^\circ$  halo show a gradually decreasing intensity as a function of scattering angle, which is

absent in our graph. This feature, however, is due mainly to the geometry of the crystal, which has been neglected in our approach. Handling these geometry factors in the same way as we did the deflection functions, it can be expected that our results will fit Greenler's at a larger angular scale. However, it is not clear if, at a large distance of  $\theta_h$ , Greenler's result is completely right since he did not take into account that, in the case of skew incidence, at the first refraction, polarization takes place, which may result in a lower intensity after the second refraction.

The color distribution of halos can be inferred from two properties: the intensity distribution of halos and the dispersion of the halo angle with the wavelength of light. In Table 3 the dispersions of the halo angle are presented between red ( $\lambda = 6563 \text{ \AA}$ ) and violet ( $\lambda = 4047 \text{ \AA}$ ), where the indices of refraction for ice are 1.307 and 1.318, respectively.<sup>14</sup> For comparison, this dispersion for the primary rainbow angle  $\theta_r$  is also included.

The comparison between the rainbow and the halos is of relevance since the intensity distribution of the former<sup>15</sup> in the Descartes approach is  $(\theta - \theta_r)^{-1/2}$ , which is identical with the intensity distributions that we obtained for parhelia and tangent arcs. The Descartes intensity distribution becomes visible if drops of all sizes contribute, so that interference effects are smeared out. Since the horizontal cross section of a flattened drop remains a circle, this is the case near the feet of a rainbow at low solar elevation. In the top of the rainbow, this is not the case, and the Airy rainbow becomes visible.<sup>16</sup>

We now compare the color distribution of different types of halo with one another and with the Descartes rainbow. Between the parhelion and the tangent arcs, no essential difference occurs in the color distribution, since for both the dispersion and the intensity distribution (for a point source) are identical. For a finite source, the colors of the tangent arcs will be somewhat paler, but the appearance of the colors remains similar. Therefore this case needs no further discussion.

When the rainbow is compared with the parhelion, there is a difference in the dispersion. But since their intensity distributions are equal, their overall appearance is similar. Indeed, close inspection of photographs reveals that they are both characterized by a broad red edge, whereas further away from the sun the colors are less pure. Because of its larger dispersion, the mixing of colors at larger scattering angles is somewhat less rapid for the rainbow, but nevertheless the general impression of its colors remains close to that of the parhelion (or to that of a tangent arc).

The circumzenithal arc may display brilliant colors, the purity of which often surpasses that of the rainbows. This is due partly to its larger dispersion, but the behavior of its intensity distributions plays a more crucial role. If integrated over the solar disk, this intensity distribution for a given color is concentrated in an angular range of only  $0.5^\circ$  (see Fig. 2),

Table 3. Dispersion of Halos and the Rainbow

	22° Halo	46° Halo	Primary Rainbow
Difference in halo or rainbow angle between $\lambda = 6563 \text{ \AA}$ and $\lambda 4047 \text{ \AA}$	0.84°	2.4°	1.7°

which is much less than its dispersion. Therefore hardly any mixing occurs among the colors, so they remain extremely pure. Because of this property of its intensity distribution, the quality of the colors is even better than that of the secondary rainbow, although the latter has an even larger dispersion ( $2.9^\circ$ ).

In contrast to the circumzenithal arc, the  $22^\circ$  halo is known for its pale coloring, also as compared with the parheliion. Indeed, commonly only near its inner edge, a brown-reddish color is visible. This feature can be explained by its extremely flat intensity distribution. Because of this, complete mixing of the colors is already reached when the scattering angle reaches the halo angle for violet, so the halo becomes white. For smaller scattering angles, some colors dominate, but only close to the inner edge of the halo is there some purity. The width of the part of the halo where some coloring is perceptible is only  $1^\circ$  or less.

Some years ago Fraser<sup>17</sup> explained the lack of color in the  $22^\circ$  halo by the small size of the generating crystals and the broad diffraction maximum of such crystals. Although this effect may also contribute to the paleness of this halo, the flat intensity distribution is probably the main cause of this feature.

### Polarization

The polarization pattern of all refraction halos shows a marked structure near the halo angle at an angular scale of  $0.1^\circ$  and  $0.5^\circ$  (the angular width of the sun). For parhelia and tangent arcs, this structure is rather similar, leading to a sharp increase in the polarization near the halo edge and a second maximum with reversed polarization, separated by  $0.5^\circ$  from the first one. With the naked eye this first maximum for red light can easily be observed at the inner edge of the halo, but for other colors it remains hidden because of the mixing of the colors. For the same reason, the second maximum cannot be observed either. However, it can be expected that the latter must be visible with monochromatic filters. Figure 7 shows that polarimetry is a sensitive means to detect parhelia, since the polarization at the two maxima are, respectively, seven and four times stronger than the maximum quantity of polarized light that should result from Fresnel refraction alone. For the tangent arcs these numbers are six and three, respectively. It must be noted that at higher solar elevations the polarization of parhelia should change somewhat because of the effects calculated by McDowell.<sup>6</sup>

For the circumzenithal arc, the polarization near the red edge is more difficult to observe since it is somewhat obscured by the overall polarization of the arc that is due to Fresnel refraction. A second reason is that the angular separation of the polarized components is rather small compared with the dispersion of the halo, whereas at  $46^\circ$  from the sun a rather strong polarization of the blue sky is present with the same direction as the one of the inner edges of the halo. Nevertheless, in February 1980 we were able to observe this polarization near the red inner edge of a bright circumzenithal arc.<sup>2</sup> The observed direction of the polarization was in agreement with the calculation.

Although the polarization of the  $22^\circ$  halo near its edge may exceed the Fresnel polarization by a factor of 4, this maximum remains weaker than that of the parhelia or tangent arcs. As far as we know, this polarization has never been observed. It may be interesting to try this, although the low intensity near

the edge of the halo makes this polarization more difficult to observe than for the tangent arcs or the parhelia.

## 9. CONCLUSION, FURTHER RESEARCH, AND APPLICATION TO VENUS

Intensity distributions, polarization distributions, and shapes have been calculated for various classes of halo by using simplified halo formulas. It is found that the intensity distribution of halos depends strongly on the degree of freedom in the generating set of crystals. The polarization calculations describe well the observed strong polarization near the inner red edge of parhelia and tangent arcs but also predict a secondary maximum of inverse polarization in the polarization distribution that is unobserved so far. The intensity distributions that we obtained offer an explanation of the difference in the color distributions of various types of halo. Finally, our formalism enables one to express the shape of halos in terms of simple functions.

Although the intensity distributions agree closely with the ones obtained by Greenler<sup>5</sup> with the Monte Carlo method, it would be useful to compare them with direct observations. This requires photographs of halos with monochromatic filters. Unfortunately, as far as we know, no such pictures exist so far. It will be interesting to take them and to measure the intensity distributions of halos.

A second intriguing test of the theory is the polarimetry of halos near their edges in monochromatic light. Such measurements may provide a sensitive test of the theory indeed.

The explanation of a halo with unusual radii is not always completely settled. Measurements of the polarization of their inner edges may sometimes provide a clue to their explanation. For an inclination of  $25^\circ$  of the pyramidal faces<sup>9</sup> of the crystals, the direction of polarization of the inner edges of the resulting  $8^\circ$  and  $17^\circ$  halos is expected to be perpendicular to the plane of scattering, just as in case of the  $46^\circ$  halo. The distances of the polarized components are predicted to be  $0.04^\circ$  and  $0.08^\circ$ , respectively. For some other halos, however, no polarization at the inner edge should occur.

Finally, a challenging project should be a search for ice crystals on Venus. If hexagonal ice crystals are present in the upper atmosphere of the planet, a sharp increase in the polarization can be expected if Venus passes the halo angle. A preferential orientation of the crystals, which should lead to tangent arcs, will result in a larger quantity of polarized light near the equator of Venus, but, because of the curvature of the planetary disk, its intensity distribution remains the same as expected for randomly oriented crystals. Thus the polarization pattern will have a smooth maximum of an angular width of about  $0.74^\circ$ , which is the solar diameter as seen from Venus. On the other hand, if parheliion-generating crystals are present, the scattering is concentrated near the poles of the planet. In this case, the curvature of the disk leads to a transformation of the intensity distribution into that of the tangent arcs. This means that two sharp peaks in the polarization will occur at an angular separation of  $0.74^\circ$ . The width of the peaks is of the order of  $0.1^\circ$ , which means that Venus passes through it in only 90 min.

Venus passes the  $22^\circ$  halo scattering angle only when it is close to inferior conjunction. This happens every 19 months. The next occasions will be in April 1985 and November 1986,

approximately. A concentrated search of narrow peaks in the polarization of Venus that are due to birefringence has still to be done.<sup>18</sup> It will be interesting to explore these opportunities.

## APPENDIX A: NOTATION

### Vectors and Planes

0, origin.

$\hat{S}_1$ , unit vector pointing to the sun; thus in the direction of the incoming light.

$\hat{S}_2$ , unit vector in the direction of the outgoing light (after two refractions in this case). The projections of  $\hat{S}_1$  and  $\hat{S}_2$  in the crystal-normal plane are indicated in Fig. 1d.

$\hat{Z}$ , unit vector pointing to the zenith.

$\hat{N}$ , unit vector in the direction of the solar normal, in the plane defined by  $\hat{S}_1$  and  $\hat{Z}$ .

Solar-normal plane: a plane perpendicular to  $\hat{S}_1$  through O.  $\hat{N}$  is in this plane.

Crystal-normal plane: any plane perpendicular to both refracting faces of the crystal.

$\hat{P}$ , axial vector. This is the unit vector perpendicular to the crystal-normal plane (in the case of halos formed by single external refraction, this vector is the commonly chosen normal to the reflecting plane).

$\hat{P}'$ , projection of  $\hat{P}$  in the solar-normal plane.

$\hat{T}$ , unit vector in the direction of the light path in the crystal.

$\hat{X}$ , unit vector along the optical axis of the crystal. For the 22° halo group,  $\hat{X}$  coincides with  $\hat{P}$ .

Scattering plane: plane defined by  $\hat{S}_1$  and  $\hat{S}_2$ .

Solar almucantar: horizontal plane through the sun.

Solar vertical: vertical plane through the sun.

### Angles

A, angle between the refracting faces, so  $A = 60^\circ$  for the 22° halo group and  $A = 90^\circ$  for the 46° halo group.

$\theta$ , scattering angle with respect to the sun; thus  $\angle \hat{S}_1 \hat{S}_2$ . This is  $\Delta$  in Humphrey's notation.

$\phi$ , scattering azimuth with respect to the solar vertical; thus the angle between the planes  $\hat{S}_1 \hat{S}_2$  and  $\hat{S}_1 \hat{Z}$ .

$\phi'$ ,  $\phi - q$  (see the definition of  $q$  below).

$h$ ,  $\angle \hat{P}' \hat{P}$ . This angle determines the position of the crystal-normal plane with respect to the sun. Many authors use its complement,  $90^\circ - h \equiv \angle \hat{P} \hat{S}_1$ , denoting it by  $\theta$ . In our case,  $h$  is more convenient.

$q$ ,  $90^\circ - \angle \hat{P}' \hat{N}$ , angle between the projection of the axial vector in the solar-normal plane and the crossing line of the solar normal plane with the horizon.

$i$  and  $i'$ , angle of incidence at the entry face and angle of refraction at the exit face, respectively, projected in the crystal-normal plane.

$r$  and  $r'$ , angle of refraction at the entry face and angle of incidence at the exit face, respectively, projected in the crystal-normal plane.  $r + r' = A$ .

$D$ , projected deviation; thus the projection of  $\theta$  in the crystal-normal plane.

$D_m$ , minimum deviation; this is the minimum value of the function  $D(\alpha, h)$  for a fixed  $h$ .

$i_m$  and  $r_m$ ,  $i$  and  $r$  at minimum deviation. Here  $i_m = i'_m$ ,  $r'_m = r$ ,  $i_m = (D_m + A)/2$ .

$\theta_h$ , halo angle; this is the absolute minimum of the function  $\theta(\alpha, h)$ .  $\theta_h = \theta(0, 0)$ .

$i_h$  and  $r_h$ ,  $i$  and  $r$  at halo angle.

$\alpha$ ,  $i - i_h$ .

$\alpha_0$ ,  $\alpha$  at  $h = 0$  for circumzenithal or Parry arcs.

$\Sigma$ , solar elevation; thus  $\angle \hat{Z} \hat{N}$ .

$s$ , solar semidiameter,  $s = 0.25^\circ$ .

$\gamma$ , angle between the light path in the crystal and the optical axis of the crystal; thus  $\gamma = \angle \hat{T} \hat{X}$ .

$\Delta\theta_h$ , difference in halo angle between the ordinary and extraordinary refracted rays.

$\theta_{\text{edge}}$ , halo-edge scattering angle, which is the smallest value of  $\theta_h - s$  for a given halo, taking both polarizations into account. This angle represents the scattering angle of the inner edge of a halo for a finite sun.

### Scalars

$N$ , number of crystals giving rise to scattering in a given solid angle.

$I$ , intensity of the outgoing ray (normalized units).

$I_1$  and  $I_2$ , intensity of the polarization component in the scattering plane (that is, the plane defined by  $\hat{S}_1 \hat{S}_2$ ) and perpendicular to it, respectively.  $I \equiv I_1 + I_2$ .

$I_{\text{pol}}$ , quantity of polarized light,  $I_1 - I_2$ .

$\bar{I}$ ,  $\bar{I}_1$ , etc., the same after integration over the solar disk.

$P$ , degree of polarization. If no background intensity  $I_B$  is present,  $P = -I_{\text{pol}}/I$ . Otherwise,  $P = -I_{\text{pol}}/(I + I_B)$ .

$n$ , index of refraction. For ice,  $n = 1.31$  for yellow light.

$n'$ , Bravais refractive index.  $n' = [(n^2 - \sin^2 h)/(\cos^2 h)]^{1/2}$ .

$n_o$  and  $n_e$ , index of refraction for ordinary and extraordinary refracted rays, respectively.

$\delta n \equiv n_e - n_o$ , birefringence of ice. For visible light,  $n_e - n_o = 0.0014$ .

$n_{\text{eff}}$ , effective index of refraction of extraordinary rays,  $n_{\text{eff}} = n_o + \sin \gamma (n_e - n_o)$ .

## ACKNOWLEDGMENT

I thank Walter Tape for his most valuable comments when refereeing this paper.

## REFERENCES

1. G. P. Können, "Polarization of haloes and double refraction," *Weather* **32**, 467-468 (1977).
2. G. P. Können, *Polarized Light in Nature* (Cambridge U. Press, Cambridge, to be published); (Dutch ed., Thieme, Zutphen, the Netherlands, 1980).
3. R. White, "Intensity plots of the parhelia," *Q. J. R. Meteorol. Soc.* **103**, 169-175 (1977).
4. A. B. Fraser and G. J. Thompson, "Analytic sun pillar model," *J. Opt. Soc. Am.* **70**, 1145-1148 (1980).
5. R. Greenler, *Rainbows, Halos and Glories* (Cambridge U. Press, Cambridge, 1980).
6. R. S. McDowell, "The formation of parhelia at higher solar elevations," *J. Atmos. Sci.* **31**, 1876-1884 (1974).
7. R. White, "Deviation produced by anisotropic prisms," *J. Opt. Soc. Am.* **70**, 281-287 (1980).
8. G. P. Können and J. H. de Boer, "Polarized rainbow," *Appl. Opt.* **18**, 1961-1965 (1979).
9. W. J. Humphreys, *Physics of the Air* (Dover, New York, 1964).
10. R. A. R. Tricker, *Introduction to Meteorological Optics* (Elsevier, New York, 1970).

11. W. Tape, "Analytic foundations of halo theory," *J. Opt. Soc. Am.* **70**, 1175-1192 (1980).
12. W. Tape, "Folds, pleats and halos," *Am. Sci.* **70**, 467-474 (1982).
13. For the properties of the Dirac delta function and the Heaviside step function see, e.g., A. Messiah, *Quantum Mechanics* (North-Holland, Amsterdam, 1965), Vol. I.
14. P. V. Hobbs, *Ice Physics* (Clarendon, Oxford, 1974), p. 202.
15. H. C. van de Hulst, *Scattering of Light by Small Particles* (Wiley, New York, 1957), p. 245.
16. A. B. Fraser, "Why can the supernumerary bows be seen in a rain shower?" *J. Opt. Soc. Am.* **73**, 1626-1628 (1983).
17. A. B. Fraser, "What size of ice crystals causes the halo?" *J. Opt. Soc. Am.* **69**, 1112-1118 (1979).
18. J. Veverka, "A polarimetric search for a Venus halo during the 1969 inferior conjunction," *Icarus* **14**, 282-283 (1971).



Plate I. (Alistair B. Fraser, p. 1626). The top of a rainbow, which shows two supernumerary bows. © Alistair B. Fraser.



Plate II. (G. P. Können, p. 1629). Birefringence of ice crystals caused a remarkable polarization of the parhelion. Rotating a polarizer before the eye changes its position with respect to the sun by  $0.11^\circ$  (photographed by A. Tramper).

